Photoresponsive hierarchical ZnO-PDMS surfaces with azobenzene-polydopamine coated nanoparticles for reversible wettability tuning

Christine Kallweit*[1], Matthias Bremer[1], Daria Smazna[2], Torben Karrock[1], Rainer Adelung[2] and Martina Gerken[1]

Address: [1]Chair of Integrated Systems and Photonics, Institute of Electrical Engineering and Information Technology, Kiel University, Kaiserstrasse 2, 24143 Kiel, Germany and [2]Chair of Functional Nanomaterials, Institute for Materials Science, Kiel University, Kaiserstrasse 2, 24143 Kiel, Germany

Email: cka@tf.uni-kiel.de

* Corresponding author

Abstract

Azobenzene-bearing surfaces are promising for light-controlled wettability switching in microfluidic systems. We investigate the wettability and stability of flat glass, flat polydimethylsiloxane (PDMS) and hierarchical ZnO-PDMS surfaces functionalized with azobenzene bearing polydopamine coated nanoparticles (Azo-PDA-NP). We analyse the stability of the contact-angle switching when using new droplet locations for each measurement and for using the same droplet location with compressed-nitrogen drying between measurements. For flat glass surfaces we observed a wettability change of 15° and 60° for spin-coating and drop-casting deposition of the Azo-PDA-NP,

respectively. For the PDMS samples, 60° contact-angle change are obtained, but these surfaces show degradation for repeated switching cycles. In contrast the hierarchical ZnO-PDMS surfaces exhibit a wettability switch of 50° and no degradation for five switching cycles at the same droplet location. We captured water drops during ultra-violet (UV) irradiation on video and obtained a one-sided flowing motion with a speed of 1.9 µm/s. Contact-angle hysteresis measurements show that the minimum criterion for droplet movement is fulfilled for the Azo-PDA-NP functionalized hierarchical ZnO-PDMS surfaces.

Keywords

Azobenzene; hierarchical surface; photo responsivity; smart surface; wettability change

1. Introduction

Smart surfaces, i.e., stimuli-responsive materials at surfaces, are of high interest as control elements for microfluidic systems. Due to the change of their macroscopic properties by external stimuli they may be applied in lab-on-chip devices, for biological, or for chemical tests. Temperature, pH, chemicals, electric current, or light may serve as external stimuli [1-3]. The prevailing stimulation mechanism is light. In contrast to the other stimuli, light offers noncontact operation and allows for a precise control in parameters such as wavelength, intensity, and direction [4-11]. From the technological point of view, it is also easier to miniaturize light setups [8,9].

ZnO and TiO_2 are inorganic oxides that exhibit a light-triggered transition from the hydrophobic initial state to a hydrophilic state via ultra-violet (UV) irradiation. The recovery time to the hydrophobic state is too long (sometimes up to days) for being practical, though [12]. Extensive investigations were conducted concerning different morphologies and their effect on wettability behaviour [8-20]. The tunability process is based on the competition of the thermodynamically favourable behaviour of oxygen adsorption and a UV-induced kinetical process, in which photogenerated defective sites increase the affinity of water absorption on the surface [13].

Organic materials composed of chromophores are a different class of materials exhibiting reversible switching processes. Illumination with the appropriate wavelength causes distinct changes in their molecular structure. Binding these molecules to surfaces allows for altering the surface properties and thus for wettability changes [21,22]. Azobenzene and its derivatives are the most studied molecule class of this type [9,10,23-27]. UV irradiation transforms the thermodynamically stable elongated *trans*-isomer into the shortened *cis*-isomer [23,28-30]. Exposure to visible light (especially blue or green light) returns the molecule to the initial *trans*-state. This isomerization process may be verified by UV-spectra measurements. Surfaces functionalized with azobenzenes show a higher water contact angle (hydrophobic state) in the *trans*-state, because a lower surface energy and a small dipole moment prevail. If the *cis* form is present on the surfaces, the water contact angle is lowered due to a larger surface energy and a higher dipole moment [23]. The wettability of these azobenzene systems depends on the morphology. Flat surfaces functionalized with azobenzenes have a light-induced change in water contact angle of only

~10° [24,31]. To enhance switching efficiency nano- and microporous surfaces were functionalized with azobenzenes demonstrating contact-angle changes of up to ~150° [32,33]. Also, a combination of azobenzenes with TiO_2 was reported [34] for creating such superhydrophobic to superhydrophilic states.

Many different techniques are available for the fabrication of organic molecule bearing surfaces. These include the formation of self-assembled monolayers, linkages with long alkyl chains [4,35-37] as well as polymer approaches [4,25,38]. The use of mussel-inspired adhesion methods with polydopamine, a facile multifunctional method to modify surfaces, was recently reported [39-42]. Polydopamine is created by oxidative polymerization of dopamine-hydrochloride in buffered aqueous solutions with a pH of 8.5. These systems open catechol binding sites, which provide a basis for several different interactions and reactions, such as π-π stacking, van der Waals forces, coordination, and covalent linking [43].

J. Zhang et al. [44] synthesize SiO_2 nanoparticles, coat these with polydopamine and subsequently functionalize the particles with fluorinated azobenzenes. Processing these functionalized particles on surfaces they demonstrate superhydrophobicity and contact-angle changes of ~15°.

Inspired by the functionalization method by J. Zhang et al. [44] we investigate the surface stability of different types of flat and structured functionalized surfaces to repeated droplet placement and switching cycles. For using functionalized surfaces in practical microfluidic systems, the stability to droplet movement is an important requirement and this study aims to bring functionalized surfaces closer to application. We synthesize SiO_2 nanoparticles

(NP), coat them with polydopamine and link an azobenzene derivative with amine functional groups described by Groten et al. [25] to the catechol binding sites. The process is depicted in Fig. 1 (a). The functionalized nanoparticles subsequently are deposited on different types of substrates. As summarized in Fig. 1 (b) we investigate functionalized flat glass and polydimethylsiloxane (PDMS) substrates as well as hierarchical ZnO-PDMS substrates. The hierarchical ZnO-PDMS substrates (sample 3 and 4) are formed by first dipcoating hierarchical ZnO onto a glass substrate. These ZnO surfaces show nanospiked sea-urchin-type 3D-structures. The core sizes range from 5-10 µm, the nanospikes appear as flat rods with a width of 1 µm at the bottom and reduce to few nanometers at the tip [45,46]. Next, the hierarchical ZnO-glass substrate is coated with PDMS by pouring on liquid PDMS, curing the PDMS, and separating off the access PDMS. The resulting samples are analyzed with scanning electron microscopy, UV spectroscopy, contact-angle measurements and video capture.

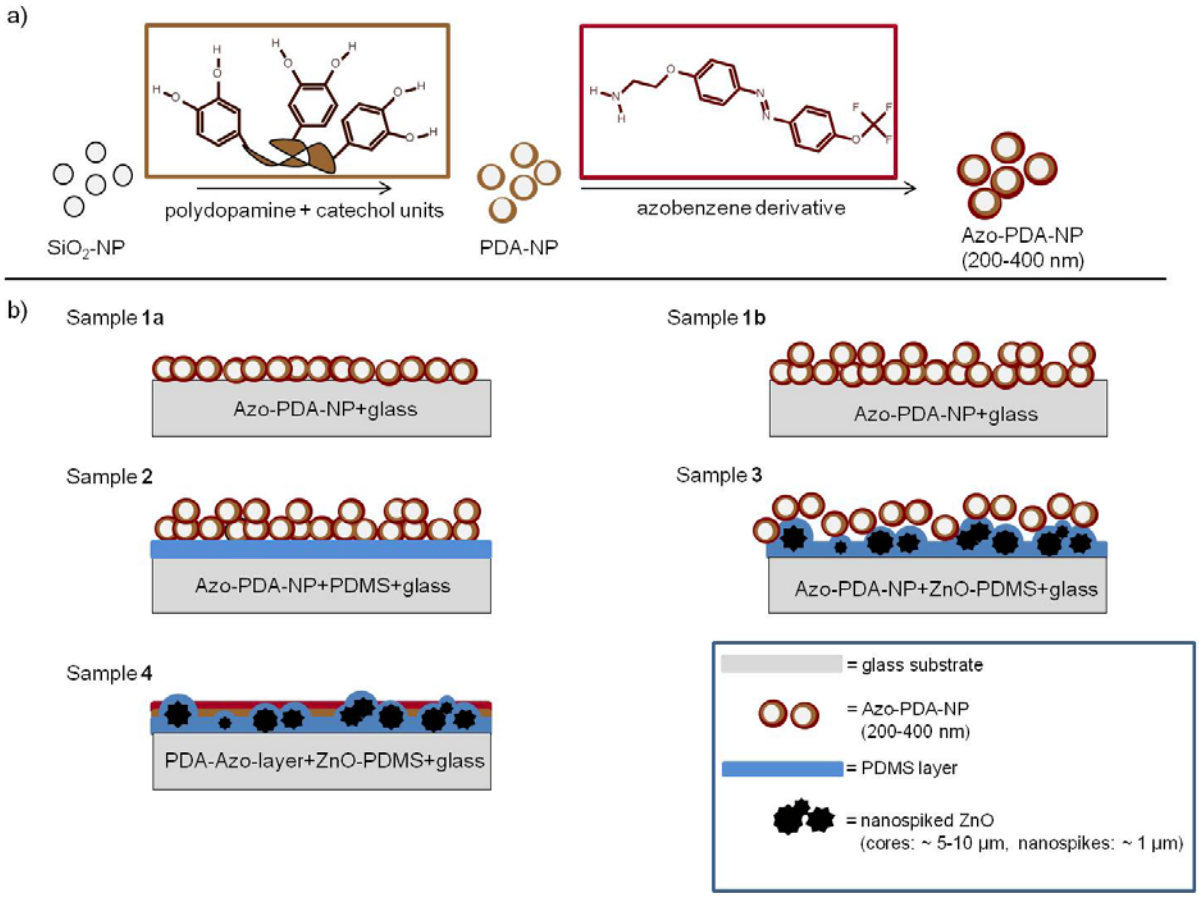

Fig. 1. (a) SiO_2 nanoparticles (NP) are functionalized with polydopamine (PDA) and azobenzene (Azo) to obtain azobenzene-polydopamine functionalized nanoparticles (Azo-PDA-NP). (b) Five types of photoresponsive samples are fabricated – four types are covered with Azo-PDA-NP, the last one has a polydopamine-azobenzene layer without nanoparticles for reference: 1a) flat glass, spin coated; 1b) flat glass drop coated; 2) flat PDMS-glass drop coated; 3) hierarchical PDMS-layered ZnO surface drop coated; 4) hierarchical PDMS-layered ZnO surface drop coated.

2. Experimental

2.1. Nanoparticle synthesis and coating with polydopamine

Silica nanoparticles with a diameter of 200-400 nm were prepared according to the following altered Stoeber procedure [47,48]. First ethanol (10 mL), ammonia water solution (0.25 mL), and deionized water (5.4 mL) are transferred into a glass beaker and stirred for 10 minutes. Then tetraethyl orthosilicate (TEOS; Sigma Aldrich) is rapidly added (2 mL). The solution is stirred for three hours at room temperature. Collection of the developed SiO_2-nanoparticles is done after several washing cycles in ethanol by centrifugation. Then the particles are dried in an oven (100°C, 60 min).

For coating, dopamine hydrochloride (60 mg; Sigma Aldrich) is dissolved in a Tris-HCl buffer solution (10 mM, 30 mL, pH 8.5; Jena Bioscience GmbH) and stirred for 15 minutes. Afterwards the dried SiO_2-nanoparticles are added to the buffered solution. After 24 hours the polydopamine-coated nanoparticles are subjected to washing cycles with ethanol and deionized water. Isolation is performed via centrifugation. The obtained particles are stored in ethanol (8 mL).

2.2 Nanoparticle functionalization with azobenzene and layer deposition on glass (Sample types 1a and b)

The polydopamine coated nanoparticles are dispersed in an ethanolic azobenzene solution (10.0 mg/mL of 2-[4-(4-Trifluoromethoxy phenylazo) phenoxy] ethanamine [25]; Squarix GmbH). Two different deposition processes are employed – a drop casting method (100µL) and a spin-coating process (100µL, 40 sec, 1000 rpm with 800 rpm/sec). Before casting, the substrates (2.5

cm x 2.5 cm) are sonicated in isopropanol for 5 minutes. After the deposition processes the samples are annealed at 120°C for approximately 4 h. Finally, the samples are carefully rinsed with deionized water to remove unbound azobenzenes and particles.

2.3 Fabrication of flat PDMS substrates and layer deposition (Sample type 2)

Glass substrates are sonicated in acetone and isopropanol (for 7 min each). Afterwards they are dehydrated for 10 min at 160°C on a hotplate. For the PDMS casting layer Sylgard 184 and the corresponding curing agent purchased from Dow Corning Corporation are mixed in a ratio of 8:1 for 20 minutes, degassed and spin coated (60 sec, 1500 rpm with 300 rpm/sec) onto the glass samples. Curing is performed in an oven at 130°C for at least 1 h. For casting the substrates with functionalized nanoparticles the samples are immersed in isopropanol for 3 minutes, dried under nitrogen flow and activated by plasma etching (8 sccm O_2, 50 W and 30 sec). Then the solution with azobenzene functionalized nanoparticles is added dropwise. Annealing and cleaning is performed identical to the former flat glass substrates. Note that the casting process is challenging. The Azo-PDA-NP solution concentrated onto the PDMS surface non-uniformly.

2.4 Fabrication of photoresponsive hierarchical structured ZnO-PDMS surfaces with nanoparticles (Sample type 3)

Synthesis and fabrication of the nanospiked sea-urchin-type ZnO is described elsewhere [45,46]. ZnO itself undergoes a mechanism analogous to photocatalysis due to UV-light irradiation [12,13]. Nevertheless, some ZnO films show UV-durable superhydrophobic and superoleophobic properties, due to the

combination of certain composites [49]. When combining inorganic oxides with azobenzene it is a challenge to differentiate between the two possible switching processes – the photocatalytic process of the ZnO and the azobenzene isomerization. PDMS can serve as suppressor for the photocatalytic event of ZnO [50]. Normally such ZnO-PDMS nanocomposite coatings are fabricated by dispersing ZnO nanoparticles and PDMS in solvents [51-54] with subsequent casting onto the provided surfaces. We use a different technique, in which we coat the ZnO with PDMS.

To create ZnO-PDMS hybrid layers, Sylgard 184 and the corresponding curing agent (Dow Corning Corperation) are mixed and degassed such as described before. The ZnO-layered glass substrates are cleaned in acetone and isopropanol, dried with nitrogen flow, and positioned into Teflon bordered casting molds. Then the PDMS liquid matrix is poured over pristine ZnO samples and cured in an oven for 2 h at 100 °C. Finally, the hardened PDMS is carefully separated from the hybrid ZnO-PDMS layer. A PDMS-coated nanostructured ZnO surface remains on the glass substrate (supporting information Fig. S1 gives scanning electron microscopy images of a ZnO-PDMS sample and the removed PDMS negative). UV-light irradiation induces no change in hydrophobicity (supporting information Table S1 contact-angle measurement). Finally, these samples are functionalized as described for the flat PDMS substrates with the steps of cleaning, activation via plasma etching, casting (drop method), annealing, and washing.

2.5 Fabrication of photoresponsive hierarchical structured ZnO-PDMS surfaces without nanoparticles (Sample type 4)

This hierarchical ZnO-PDMS surface is fabricated like sample 3. The functionalization process is performed with a solution of 2-[4-(4-Trifluoromethoxy phenylazo) phenoxy] ethanamine and polydopamine, but without nanoparticles. The concentrations are identical to the solution described above.

2.6 UV-spectra monitoring

Photoisomerization experiments of the azobenzene modified substrates are carried out with a Perkin Elmer UV/Vis spectral photometer Lambda 650. Spectra are taken before and after UV irradiation (30 sec, 365 nm, Nichia-LED, NCSU033B) to prove isomerization and hence a successful azobenzene binding. For back-isomerization a blue LED (60 sec, 448 nm, Luxeon, Rebel LXML PR01 0500) serves as light source.

2.7 Contact-angle measurements

Water is the most relevant liquid for practical applications [25]. Thus, we investigate the wettability change of water droplets. The wetting experiments are performed with an OCA50AF (Dataphysics, Germany) applying the Laplace-Young fitting method. Results are average values of the contact angles on both sides of the imaged droplet. To examine the surface stability three water droplets with a volume of 5 µL are placed onto the surface and the initial contact angles are measured. After the contact-angle measurement the water droplets are removed and the surface is dried with compressed nitrogen. Then the surface is irradiated with the UV LED (365 nm, 3.3 mW/cm^2, Nichia), three new drops are put onto the initial spot sites and three additional drops are placed at new sites. The contact angles of the six water droplets are monitored. Next the

drops are removed again, the surface is dried and irradiated with blue light (448 nm, 3.0 mW/cm^2, Luxeon) completing an irradiation cycle. The contact angles are recorded as before for new drops at three new sites and the three initial sites. Overall 5 irradiation cycles are conducted. The irradiation times are 20 min for the UV-LED and 40 min for the blue LED (supporting information Fig. S2 gives wettability measurements with varying irradiation times). The contact angles are measured after 30 seconds of drop setting, respectively. Measurements regarding the advancing and receding contact angles are also accomplished using an OCA50AF with the software SCA 20. We examined the hysteresis values for water drops (total volume of 4 and 8 µL) concerning the three states (initial state (*trans*1)), after UV irradiation (*cis*1) and after blue light irradiation (*PSS*) on 4 to 5 different substrate locations.

2.8 Scanning electron microscopy (SEM)

For SEM images a gold layer of 40 nm is vaporized onto all samples. High resolution images of the different surfaces are taken with a scanning electron microscope (Helios Nanolab 600 from FEI). Sideview images are captured with a tilt angle of 52°.

3. Results and Discussion

3.1 Investigations: surface appearance (1), isomerization (2) and wettability (3)

Table 1 lists all the investigated samples. The surface morphology and the contact-angle change for deionized water induced by UV and blue light irradiation are analysed. Here, two different methods are applied in the contact-angle measurement – the first method uses a new location for contact-angle measurement after each illumination step, the second method uses the same location with removal of the water drop and compressed-nitrogen drying of the surface. The second approach induces a significantly larger mechanical stress to the surface and is indicative for the stability of the surface in a practical microsystem with moving droplets. Finally, we present a contact-angle hysteresis analysis and additionally employed video capture of the drops during illumination to determine, if light-induced motion of a water droplet with a certain volume is possible in principle.

Table 1

Prepared sample types with employed casting processes and analysis methods.

Sample	Schematic	Casting method	Analysis		
			SEM[a]	UV[b]	θ_{trans}[c] / θ_{cis}[d]; $\Delta\theta$[e]; Stability
1a	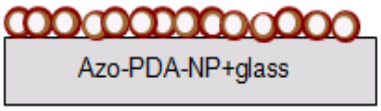	Spincoating **w** nanoparticles	-	Yes	97° / 82°; 15°; **No**
1b	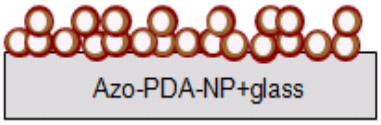	Drop method **w** nanoparticles	Yes	-	130° / 70°; 60°; **No**
2	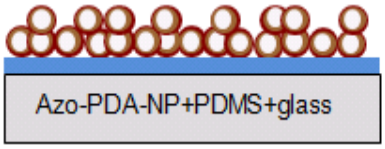	Drop method **w** nanoparticles	Yes	Yes	112°/ 52°; 60°; **No**
3	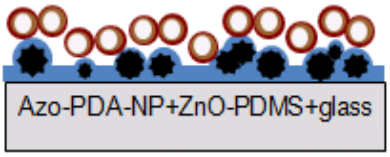	Drop method **w** nanoparticles	Yes	-	129° / 79°; 50°; **Yes**
4	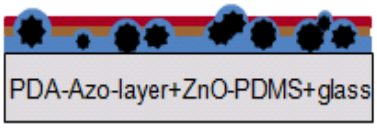	Drop method **w\o** nanoparticles	Yes	-	92°/ n. a. n. a.; **No**

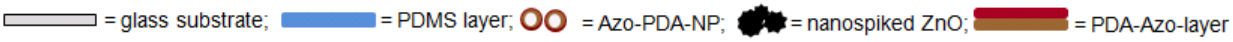

[a]Scanning electron microscopy, [b]UV-spectroscopy, [c]Contact angle of *trans*-state, [d]Contact angle of *cis*-state, [e]Wettability change: contact-angle difference between *trans*- and *cis*-state

First, we present scanning electron microscopy (SEM) images of the surface structure of a pristine ZnO glass sample and the fabricated surfaces. Fig. 2 depicts SEM images of pristine ZnO. The structure (Fig. 2 (a) and (b)) consists of nanospikes on cores and free glass interspaces. A closer look at these images reveals a further nanostructure. After coating with PDMS this remaining structure possibly serves as docking device for the Azo-PDA-NP (supporting information Fig. S1 SEM images of ZnO-PDMS sample and negative replica).

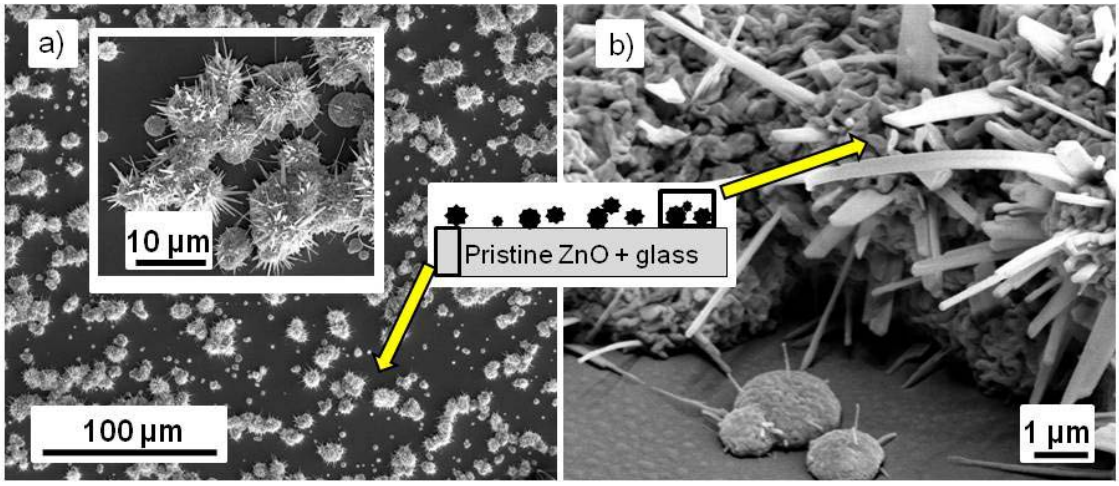

Fig. 2. SEM images of pristine nanospiked sea-urchin-type ZnO; (a) top view, (b) side view (52° tilt angle).

Fig. 3 (a)-(c) pictures the results of the samples 1b (Azo-PDA-NP+glass; drop method), 2 (Azo-PDA-NP+PDMS+glass) and 3 (Azo-PDA-NP+ZnO-PDMS+glass). In all cases the functionalized nanoparticles are visible. The flat PDMS sample 2 (Fig. 3 (b)) shows a larger density of nanoparticles, while the glass sample 1b (Fig. 3 (a)) has aggregations with free interspaces. This difference in surface appearance is due to the challenging casting process concerning the PDMS sample (see experimental section). The functionalized ZnO-PDMS surface (sample 3; Fig. 3 (c)) exhibits beside the nanoparticles a

matrix related layer. Also, the interspaces of this surface seem to be filled with this matrix. We assume the exact surface composition plays a major role in the formation of the embedment film. Fig. 3 (d) depicts the SEM results of sample 4 (PDA-Azo-layer+ZnO-PDMS+glass). The surface is completely covered with a smooth layer.

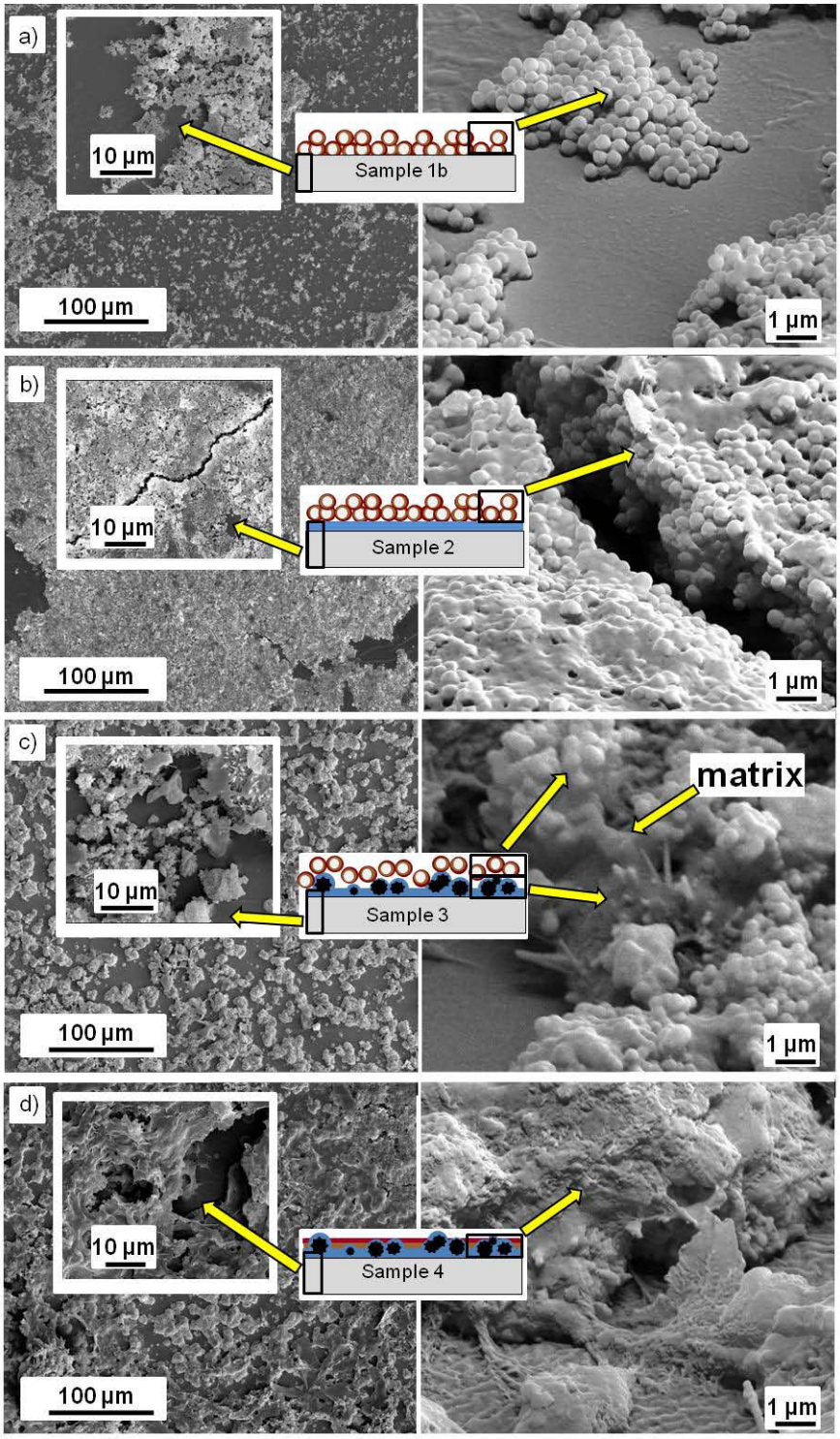

Fig. 3. SEM images of functionalized substrates: (a) glass sample 1b with nanoparticles; (b) flat PDMS sample 2 with nanoparticles; (c) ZnO-PDMS sample 3 with nanoparticles and (d) ZnO-PDMS sample 4 without nanoparticles; left images: top view, right images: side view (52° tilt angle).

Next, the azobenzene attachment via catechol units onto flat surfaces is verified with UV-spectra measurements before and after UV-light irradiation. UV-light isomerizes azobenzene and this leads to a large change in the absorbance bands [28]. Fig. 4 shows the UV-Vis spectra of a sample type 1a and sample type 2. One observes the isomerization process and that it is reversible. Both initial *trans*-states are characterized by an intensive absorbance band at 340 nm known as π→π* transition. Irradiating the samples with UV-light for 30 sec leads to decrease in π→π* transition. Simultaneously new bands appear – at 445 nm for sample 1a (Fig. 4 (a)) and at 438 nm for sample 2 (Fig. 4(b)) – attributed to the n→π* transition. Hence, it is demonstrated that isomerization occurs promoting the *cis*-state. Using blue light illumination for 60 sec the *cis*-form undergoes back-isomerization to the *trans*-state, leading back to the initial curve. The influence of the substrate type on the isomerization process is negligible. The observed difference in absorption is due to the utilized casting methods. Sample 2 exhibits more azobenzene functionalized PDA-NP because of the drop casting method. Additionally, the PDMS substrate exhibits a surface enlargement induced by the plasma etching process. The rougher PDMS offers more binding sites for the Azo-PDA-NP than glass, leading to increased azobenzene denseness and a higher absorption.

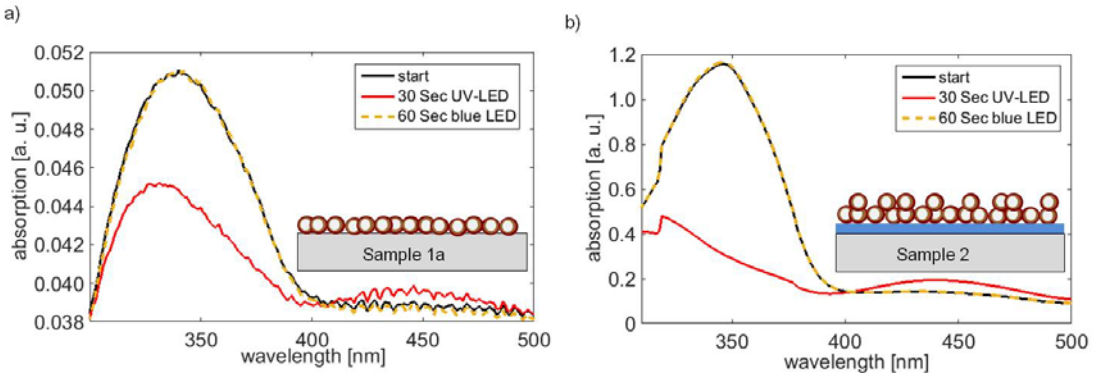

Fig. 4. UV spectra: (a) glass substrate 1a and (b) flat PDMS substrate 2 casted with Azo-PDA-NP. Initial state: black solid line; *cis*-state (after UV-light irradiation for 30 sec): red solid line, and *trans*-state (after blue light irradiation for 60 sec): yellow dashed line.

In the wettability experiments we conduct two approaches – placing the droplets on the same site after each irradiation and using a new location after irradiating. Fig. 5 (a)-(c) shows the contact-angle change of samples 1a, 1b, and 3 during 5 irradiation cycles. Using the same locations after every irradiation step one can see that for sample 1a (Fig. 5 (a); grey dashed line) the change in wettability continuously reduces. This functionalized surface obviously suffers from degradation events. In contrast, for using new locations (black line) leads to a constant contact-angle change from 97° ± 2° to 82° ± 2°, averaged 15°. This difference value is comparable to the results shown by J. Zhang et al. who also used new locations after each irradiation cycle [44,55]. We attribute the fact that our absolute contact-angle values are 50° lower to the difference in azobenzene derivative, nanoparticle content, and casting parameters.

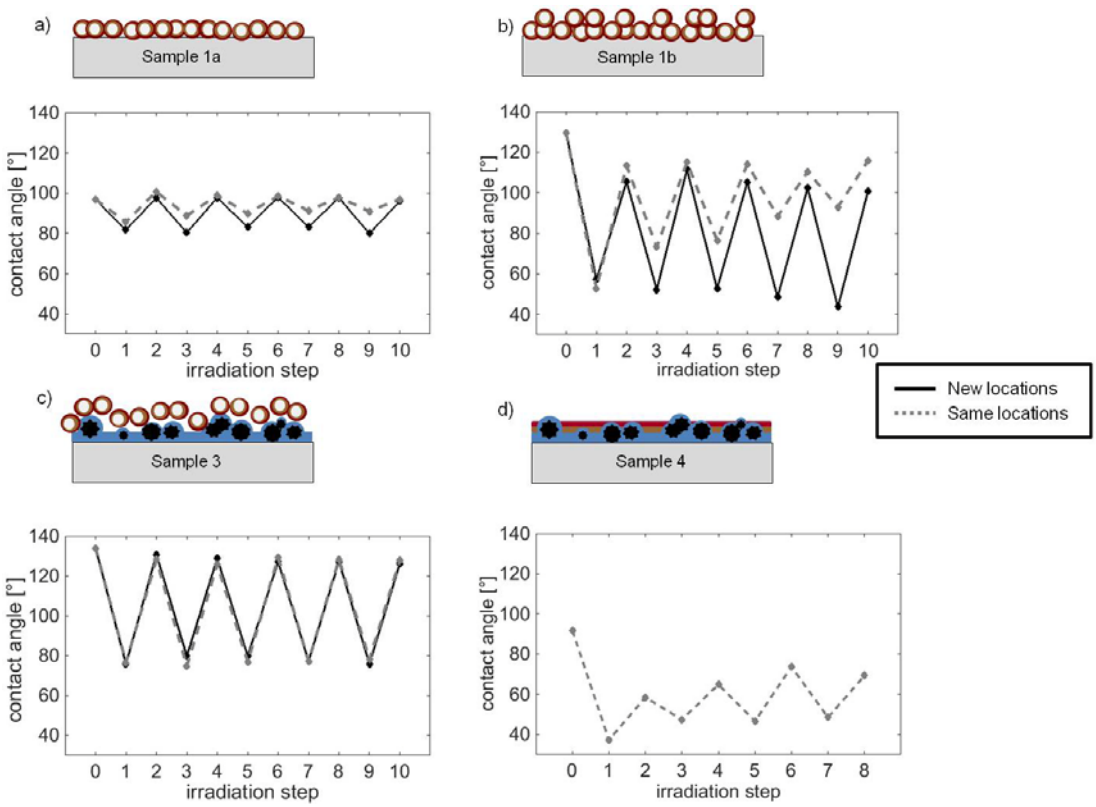

Fig. 5. Contact-angle change of functionalized substrates: (a) sample 1a; (b) sample 1b; (c) sample 3 and (d) sample 4 during irradiation steps (for UV illumination: 20 minutes, blue light illumination: 40 minutes).

We attribute the degradation when using the same site to material loss caused by mechanical stress induced by water droplet removal and surface drying with compressed nitrogen after every single measured contact angle. Thus, the approach of using the same site for repeated measurements is indicative of the surface stability.

By changing the casting process from spin coating to the drop method an enhanced contact-angle change is achieved. For sample 1b (Fig. 5 (b)) we observe a wettability difference of 60°. Using the same locations for contact-angle measurements again leads to a reduction of switching efficiency (Fig. 5 (b): grey dashed line). With every irradiation step the wettability change

decreases. From the second approach of using new locations (Fig. 5 (b): black line) it can be assumed that the surface degrades also due to irradiation with UV- or blue light. The high contact-angle value constantly reduces and never reaches the start value of 130°. The standard deviation for the *trans*-state amounts to ± 5° and for the *cis*-state to ±18°. The *trans*-form is the preferred state, because it is thermodynamically stable. So the standard deviation is only influenced by the density of present molecules and surface structure. In addition to this the deviation for the *cis*-state is also caused by the irregular irradiation due to the shadowing of the surface structure. This leads to uneven amounts of switched molecules over the observed locations and the higher standard deviation in the contact angles. We also subjected sample 2 (Azo-PDA-NP+PDMS+glass) to wettability studies and detected a wettability change of about 60°. But these surfaces also suffered from degradation events, as the samples 1a and 1b. The functionalized flat PDMS samples did not show a wettability change at the same location in a second switching process. We conclude that combining the mussel-inspired adhesive polydopamine azobenzene concept with flat substrates is not useful for the creation of stable photoresponsive surfaces. Due to the mechanical stress (drop formation - measurement - drop removal - drying by compressed nitrogen) the nanoparticles and azobenzenes lose their adhesive force causing erosion-like processes.

The wettability study for sample 3 is represented in Fig. 5 (c). The change in wettability amounts to around 50° and is thereby comparable to sample 1b with a wettability change of 60°. Furthermore, the maximum contact angle is 129°. These samples show no degradation event regardless of placing the droplet at

a new location or on the same location (grey dashed and black line). Note that the contact angle of initial *trans*-state is higher than for the *trans*-states measured afterwards. We attribute this fact to a photostationary state, where not all *cis*-isomers are excited into the *trans*-state and a low percentage remains as compact hydrophilic molecules. The standard deviations are in both states ± 4° and are comparable to literature known values.

In Fig. 5 (d) the wettability change results for sample 4 (PDA-Azo-layer+ZnO-PDMS+glass) are presented. Here, we performed a simplified measurement. Contact angles were monitored on a selfsame location of the surface and only 4 irradiation cycles were conducted. This sample with an azobenzene-polydopamine-layer, lacking nanoparticles, shows a loss of switching efficiency and a discontinuous switching event. The sample is characterized by a high wettability switch after the first irradiation step after UV-light exposure. Unfortunately, using blue light irradiation no contact angle higher than 73° is reproducible. Thus, the nanoparticles are important to increase the total contact-angle value. Without nanoparticles, the surface degrades and the adhesion between azobenzene and the ZnO-PDMS surface is less than with nanoparticles as intermediate layer. Thus nanoparticles are essential for fabricating stable photoresponsive surfaces with reproducible wettability change.

Summing up we created a photoresponsive surface with an enhanced and stable wettability change employing polydopamine functionalized nanoparticles (Azo-PDA-NP) on a hierarchical PDMS-layered ZnO surface (sample type 3). We assume the matrix observed in Fig. 3 (c) as possible reason for this good

performance. The nanoparticles are densely adhered by the polydopamine matrix and do not suffer from mechanical stress such as for the flat substrate samples 1a, 1b, and 2.

3.2 Motion of water droplet and contact-angle hysteresis

As a next step towards the practical application of these surfaces in microfluidic systems we investigate water droplet movement by UV-induced irradiation. A 5 µL water droplet is placed onto sample 3 (Azo-PDA-NP+ZnO-PDMS+glass). To induce a gradient in the UV-light irradiation we developed a setup, on which the LED is located above the droplet at a height of 10 cm and causes increasing light intensity from the right to the left edge of the surface. Videos are recorded during 30 min of irradiation. Additionally, we monitor the contact-angle change without illumination to distinguish evaporation effect.

Fig. 6 (a) shows images at selected time points obtained from the video (left: during gradual UV-light irradiation, right: without illumination). In Fig. 6 (b) and (c) images from Fig. 6 (a) are overlaid to illustrate the drop-shape change under both conditions. The diagram in Fig. 6 (d) demonstrates the contact-angle change induced via UV-irradiation (black line) and caused by evaporation without illumination (red line).

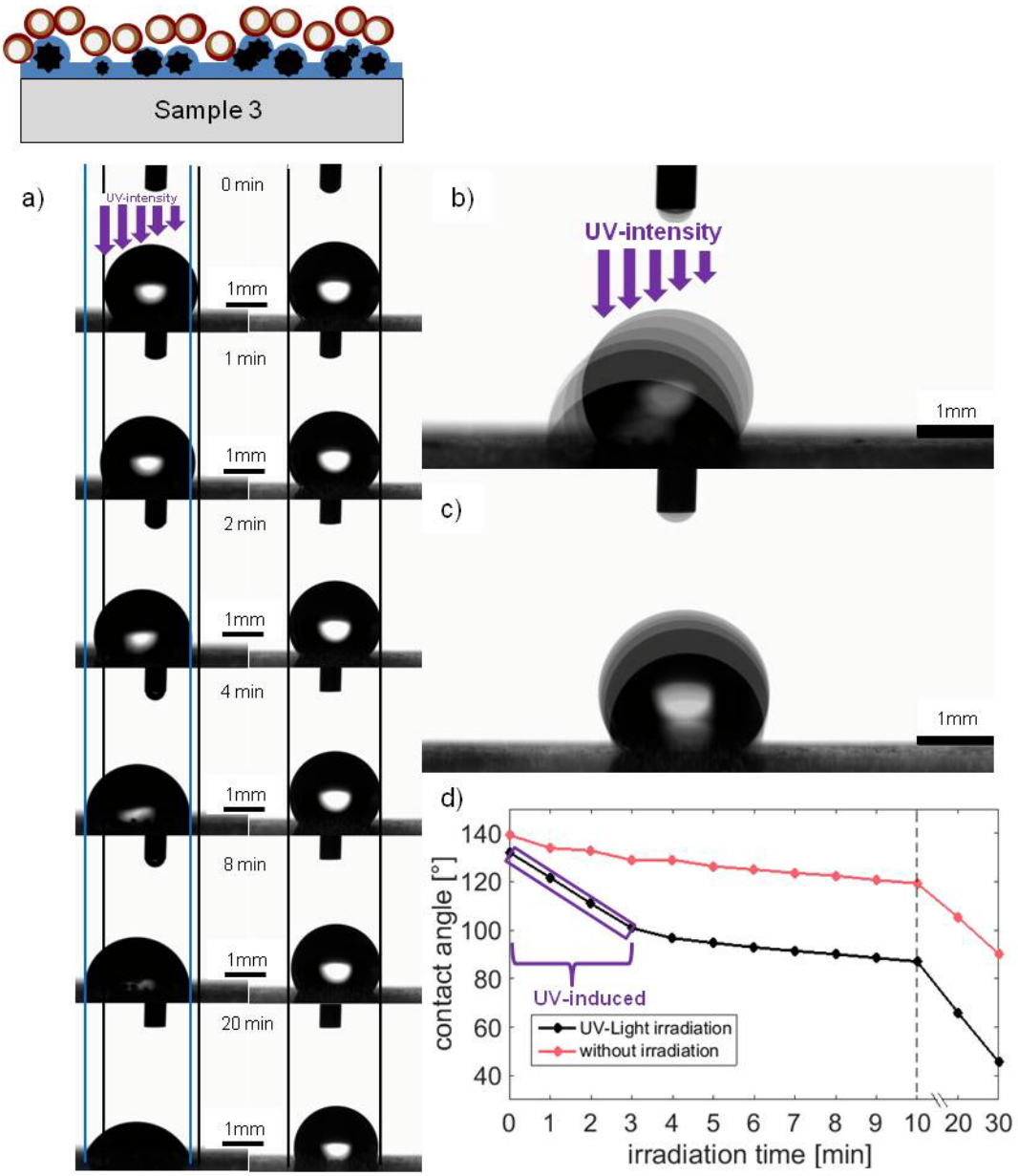

Fig. 6. (a) Selected side-view images of a water droplet on a sample 3 during gradient UV-light irradiation (left) and without illumination (right) at start time and after 1 min, 2 min, 4 min, 8 min, 20 min; (b) overlaid droplet change images during UV-light irradiation; (c) overlaid droplet change images without illumination; (d) contact-angle change over time (black solid line: during UV-light irradiation; red solid line: without illumination).

Setting the drop edges as starting points, highlighted by black lines in Fig. 6 (a), one can see that only the water droplet irradiated with UV-light performs a

flowing motion. The new drop edges are marked with blue lines (Fig. 6 (a), left images). Without illumination the droplet volume only decreases and stays within the drawn black lines (Fig. 6 (a), right images). The contact-angle change is dominated by evaporation and the contact angle is still over 120° after 10 minutes of video-capture (Fig. 6 (d), red line). The contact angle reduces linearly in the diagram. In contrast, with gradient UV illumination (Fig. 6 (d), black line) a larger reduction in contact angle is observed during the first 3 minutes of UV irradiation with a contact-angle change of 31°. Afterwards the slope is constant. After 10 minutes the contact-angle value amounts to 87°, thereby 32° less than the contact-angle value of the red graph. Hence, the contact-angle change of the first three data points is UV-induced, while the subsequent data are dominated by evaporation; exhibiting a similar slope as the red graph.

In the experiments the needle (small black box on top of each image) serves as reference. The needle has a diameter of 0.52 mm. The distance of the blue and black line on the right side of the droplet is only 0.08 mm. For the left side the motion distance is higher with a value of 0.46 mm. The process observed from the data is very slow. Other systems were published, where the movement of a drop (olive oil) was performed within seconds, with a droplet velocity of, for example, 35 µm/s [56]. We calculated a speed for our movement of 1.9 µm/s for the left droplet side. The right side is much slower with 0.3 µm/s. Monitoring the contact line change induced by UV-light irradiation, only the left side of the droplet elongates while the right side stays nearly at the same location. Overall the contact line increases from 1.8 mm to 2.5 mm, totaling about 0.7 mm. We attribute the slow process to the rearrangement of the azobenzenes linked to

the nanoparticles. Olive oil was also tested as possible liquid, but unfortunately the oil dissolved the functionalized PDA-NP from the surface.

We conducted further contact-angle hysteresis studies for sample 3 (Azo-PDA-NP+ZnO-PDMS+glass) and evaluated the minimum criterion for a guided motion of a liquid drop on photoresponsive surfaces published previously [9, 56, 57]. Hysteresis is the difference between the advancing and receding contact angle. When a liquid droplet is placed on a vertically adjusted surface, the drop is characterized by two different contact angles – the advancing and the receding contact angle. These two angles occur due to gravity, pulling the droplet to move down, and the hysteresis, keeping it in place. There are three main methods to determine contact angle hysteresis experimentally [58]. We decided to apply the sessile drop method, whereby hysteresis is detectable via liquid addition and reduction to a drop casted onto the certain balanced surface. For droplet motion the value of the *trans*-state receding contact angle – in our case two states (initial *trans*-state: $\theta_{trans\text{-rec}}$; photostationary state: $\theta_{PSS\text{-rec}}$) – has to be larger than the advancing contact angle of the *cis*-state ($\theta_{cis\text{-adv}}$). Yang et al. [9] defined the parameter K given by subtraction of the hysteresis obtained from *trans*-state ($\Delta\theta_h$ for both *trans*-states) from the contact-angle changes induced by UV-light ($\Delta\theta_s$):

$$K = \theta_{trans\text{ - rec}} - \theta_{cis\text{ - adv}} = \Delta\theta_s - \Delta\theta_h \qquad (1)$$

, where

$$\Delta\theta_s = \theta_{trans\text{ - }adv} - \theta_{cis\text{ - }adv} \qquad (2)$$

and

$$\Delta\theta_h = \theta_{trans\text{ - }adv} - \theta_{trans\text{ - }rec} \qquad (3)$$

This parameter K must be larger than 0 for the movement of a droplet. We performed two repeated measurements of the advancing and receding contact angles of the initial *trans*-state (*trans*1), the UV-induced *cis*-state (*cis*1) and the photostationary state (*PSS*) on five different substrate locations. For the water droplets we set 4 µL and 8 µL as total volumes. Table 2 lists the measured advancing and receding contact angles plus calculated K values. All K values are > 0. Thereby it is confirmed that a water droplet movement under UV-light irradiation in principle is possible.

Table 2

Investigated advancing and receding contact angles of the three states, plus the values for K, calculated by equations (1)-(3). Average values from two measurements on 5 different locations are given.

Droplet volume	θ_{trans1} [°]		θ_{cis1} [°]		θ_{PSS} [°]		K_{trans1} [°]	K_{PSS} [°]
	adv.	*rec.*	*adv.*	*rec.*	*adv.*	*rec.*		
4 [µL]	124.4	114.7	87.2	71.1	115.4	100.5	27.5	13.3
8 [µL]	117.7	103.5	84.6	64.4	119.1	103.1	18.9	18.5

Nevertheless, we only observed a flowing motion and no droplet movement in Fig. 6. This we attribute to the slow speed of the light-induced process for our samples. Here, further investigations are required.

4. Conclusion

In this study, we investigated flat surfaces and hierarchical ZnO-PDMS surfaces with azobenzene-polydopamine functionalized nanoparticles (Azo-PDA-NP) for enhanced and stable wettability changes induced via light irradiation. Firstly, we functionalized flat glass substrates and PDMS samples with Azo-PDA-NP and investigated the light triggered wettability change. These surfaces suffered from degradation events during switching cycles. On the other hand, hierarchical ZnO-PDMS surfaces functionalized with Azo-PDA-NP exhibited a stable wettability change of 50°. Functionalized hierarchical ZnO-PDMS substrates without nanoparticles decreased in switching efficiency as well as reversibility. This confirms the essential role of the nanoparticles.

Due to the stability of the nanoparticles functionalized ZnO-PDMS sample 3, it was possible to continue with investigations regarding UV-induced movement of a water droplet. Only a flowing motion instead of a droplet movement was observed though. The contact line elongates in one direction and does not simultaneously withdraw on the other side. By the means of hysteresis measurements we determined that water droplets (volume of 4 µL and 8 µL) on the surface fulfill the minimum criterion for UV-induced movement as defined by Yang et al. [9]. Next, we will include channels on the samples to promote droplet movement in a specific direction.

Acknowledgements

This work was supported by the European Research Council within the project PhotoSmart (307800).

References

[1] P.M. Mendes, Stimuli-responsive surfaces for bio-applications, Chem. Soc. Rev. 37 (2008) 2512-2529 and herein cited references.

[2] B. Xin, J. Hao, Reversibly switchable wettability, Chem. Soc. Rev. 39 (2010) 769-782.

[3] P. Cataldi, I. S. Bayer, R. Cingolani, S. Marras, R. Chellali, A. Athanassiou, A thermochromic superhydrophobic surface, Sci. Rep. 6 (2016) 27984-1 – 27984-11.

[4] S. Wang, Y. Song, L. Jiang, Photoresponsive surfaces with controllable wettability, J. Photochem. Photobiol. C: Photochem. Rev. 8 (2007) 18–29.

[5] W.R. Browne, B.L. Feringa, Light switching of molecules on surfaces, Ann. Rev. Phys. Chem. 60 (2009) 407-428.

[6] M.-M. Russew, S. Hecht, Photoswitches: From molecules to materials, Adv. Mat. 22 (2010) 3348-3360.

[7] I. Willner, S. Rubin, Control of the structure and functions of biomaterials by light, Angew. Chem. Int. Ed. Engl. 35 (1996) 367-385.

[8] R. Rosario, D. Gust, M. Hayes, F. Jahnke, J. Springer, A.A. Garcia, Photon-modulated wettability changes on spiropyran-coated surfaces, Langmuir 18 (2002) 8062-8069.

[9] D. Yang, N. Piech, S. Bell, D. Gust, S. Vail, A.A. Garcia, J. Schneider, C.-D. Park, M.A. Hayes, S.T. Picraux, Photon control of liquid motion on reversibly photoresponsive surfaces, Langmuir 23 (2007) 10864–10872.

[10] M. Chen, F. Besenbacher, Light-driven wettability changes on photoresponsive electrospun mat, ACS Nano 5 (2011) 1549-1555.

[11] A. Milionis, R. Gianuuzzi, I. S. Bayer, E. L. Papadopoulou, R. Ruffilli, M. Manca, A. Athanassiou, Self-cleaning organic/inorganic photo-sensors, ACS applied materials & interfaces 5 (2013) 7139-7145.

[12] R.-D. Sun, A. Nakajima, A. Fujishima, T. Watanabe, K.J. Hashimoto, Photoinduced surface wettability conversion of ZnO and TiO_2 thin films, Phys. Chem. B 105 (2001) 1984-1990.

[13] W.H. Hirschwald, Zink oxide: An outstanding example of binary compound semiconductor, Acc. Chem. Res. 18 (1985) 228-234.

[14] M. Li, J. Zhai, H. Liu, Y. Song, L. Jiang, D. Zhu, Electrochemical deposition of conductive superhydrophobic zink oxide thin film, J. Phys. Chem. B 107 (2003) 9954-9957.

[15] H. Liu, J. Zhai, L. Jiang, D. Zhu, Reversible wettability of a chemical vapor deposition prepared ZnO film between superhydrophobicity and superhydrophilicity, Langmuir 20 (2004) 5659-5661.

[16] E.L. Papadopoulou, M. Barberoglou , V. Zorba, A. Manousaki, A. Pagkozidis, E. Stratakis, C. Fotakis, Reversible photoinduced wettability transition of hierarchical ZnO structures, J. Phys. Chem. C 113 (2009) 2891-2895.

[17] J. Hu, Y. Sun, W. Zhang, F. Gao, P. Li, D. Jiang, Y. Chen, Fabrication of hierarchical structures with ZnO nanowires on micropillars by UV soft

imprinting and hydrothermal growth for a controlled morphology and wettability, Appl. Surf. Sci. 317 (2014) 545-551.

[18] M. Zhao, F. Shang, J. Lv, Y. Song, F. Wang, Z. Zhou, G. He, M. Zhang, X. Song, Z. Sun, Y. Wie, X. Chen, Influence of water content in mixed solvent on surface morphology, wettability, and photoconductivity of ZnO thin films, Nanoscale Res. Let. 9 (2014) 485-493.

[19] P.W. Chi, C.W. Su, B.H. Jhuo, D.H. Wei, Photoirradiation caused controllable wettability switching of sputtered highly aligned c-axis-oriented zinc oxide columnar films, Int. J. Photoenergy (2014) 1-10.

[20] A. Steele, I. Bayer, S. Moran, A. Cannon, W. P. King, E. Loth, Conformal ZnO nanocomposites coatings on micro-patterned surfaces for superhydrophobicity, Thin Solid Films 518 (2010) 5426-5431.

[21] G. Wang, J. Zhang, Photoresponsive molecular switches for biotechnology, J. Photochem. Photobiol. C: Photochem. Rev. 13 (2012) 299-309 and herein cited literature.

[22] N. Wagner, P. Theato, Light-induced wettability change on polymer surfaces, Polymer 55 (2014) 3436-3453 and herein cited literature.

[23] R. Klajn, Immobilized azobenzenes for the construction of photoresponsive materials, Pure Appl. Chem. 82 (2010) 2247-2279.

[24] X. Pei, A. Fernandes, B. Mathy, X. Laloyaux, B. Nysten, O. Riant, A.M. Jonas, Correlation between the structure and wettability of photoswitchable hydrophilic azobenzene monolayers on silicon, Langmuir 27 (2011) 9403-9412.

[25] J. Groten, C. Bunte, J. Rühe, Light-induced switching of surfaces at wetting transitions through photoisomerization of polymer monolayers, Langmuir 28 (2012) 15038-15046.

[26] S. Pan, R. Guo., W. Xu, Photoresponsive superhydrophobic surfaces for effective wetting control, Soft Matter 10 (2014) 9187-9192.

[27] Q. Shen, L. Liu, W. Zhang, Fabrication of photocontrolled surface with switchable wettability based on host-guest inclusion complexation and protein resistance, Langmuir 30 (2014) 9361-9369.

[28] H. Rau, Spektroskopische Eigenschaften organischer Azoverbindungen, Angew. Chem. 85 (1973) 248-258.

[29] H. Rau, E. Lüddecke, On the rotation-inversion controversy on photoisomerization of azobenzenes. Experimental proof of inversion, J. Am. Chem. Soc. 104 (1982) 1616-1620.

[30] D.H.M. Bandara, S.C. Burdette, Photoisomerization in different classes of azobenzenes, Chem. Soc. Rev. 41 (2012) 1809-1825.

[31] M. Han, D. Ishikawa, T. Honda, E. Ito, M. Hara, Light-driven molecular switches in azobenzene self-assembled monolayers: effect of molecular structure on reversible photoisomerization and stable *cis* state, Chem. Commun. 46 (2010) 3598-3600.

[32] H.S. Lim, J.T. Han, D. Kwak, M. Jin, K. Cho, Photoreversibly switchable superhydrophobic surface with erasable and rewritable pattern, J. Am. Chem. Soc. 128 (2006) 14458-14459.

[33] W. Sun, S. Zhou, B. You, L. Wu, Polymer brush-functionalized surfaces with unique reversible double-stimulus responsive wettability, J. Mat. Chem. A 1 (2013) 10646-10654.

[34] G. Petroffe, C. Wang, X. Sallenave, G. Sini, F. Goubard, S. Péralta, Fast and reversible photo-responsive wettability on TiO_2 based hybrid surfaces, J. Mat. Chem. A 3 (2015) 11533-11542.

[35] M. El Garah, F. Palmino, F. Cherioux, Reversible photoswitching of azobenzene-based monolayers physisorbed on mica surface, Langmuir 26 (2009) 943-949.

[36] X. Zhang, J. Shen, Self-assembled ultrathin films: From layered nanoarchitectures to functional assemblies, Adv. Mat. 11 (1999) 1139-1143.

[37] A. Ulman, Formation and structure of self-assembled monolayers, Chem. Rev. 96 (1996) 1533-1554.

[38] D.Y. Ryu, K. Shin, E. Dockenmuller, C.J. Hawker, T.P. Russel, A generalized approach to the modification of solid surfaces, Science 308 (2005) 236-239.

[39] H. Lee, S.M. Dellatoree, W.M. Miller, P.B. Messersmith, Mussel-inspired surface chemistry for multifunctional coatings, Science 318 (2007) 426-430.

[40] S. E, L. Shi, Z. Guo, Self-assembly and tribological properties of a novel organic-inorganic nanocomposite film on silicon using polydopamine as the adhesion layer, RCS Adv. 4 (2014) 948-953.

[41] Y. Liu, K. Ai, L. Lu, Polydopamine and its derivative materials: Synthesis and promising applications in energy, environmental, and biomedical fields, Chem. Rev. 14 (2014) 5057-5115.

[42] B.H. Kim, D.H. Lee, J.Y. Kim, D.O. Shin, H.Y. Jeong, S. Hong, J.M. Yun, C.M. Koo, H. Lee, S.O. Kim, Mussel-inspired block copolymer lithography for low surface energy materials of Teflon, graphene, and gold, Adv. Mat. 23 (2011) 5618-5622.

[43] J. Yang, M.A. Cohen Stuart, M. Kamperman, Jack of all trades: Versatile catechol crosslinking mechanisms, Chem. Soc. Rev. 43 (2014) 8271-8298.

[44] J. Zhang, W. Zhang, N. Zhou, Y. Weng, Z. Hu, Photoresponsive superhydrophobic surfaces from one-pot solution spin coating mediated by polydopamine, RSC Adv. 4 (2014) 24973-24977.

[45] V. Hrkac, L. Kienle, S. Kaps, A. Lotnyk, Y.K. Mishra, U. Schürmann, V. Duppel, B.V. Lotsch, R. Adelung, Superposition twinning supported by texture in ZnO nanospikes, J. Appl. Cryst. 46 (2013) 394-403.

[46] Y.K. Mishra, S. Kaps, A. Schuchardt, I. Paulowicz, X. Jin, D. Gedamu, S. Freitag, M. Claus, S. Wille, A. Kovalev, S.N. Gorb, R. Adelung, Fabrication of macroscopically flexible and highly porous 3D semiconductor networks from interpenetrating nanostructures by a simple flame transport approach, Part. Part. Syst. Charact. 30 (2013) 775-783.

[47] W. Stöber, A. Fink, E.J. Bohn, Controlled growth of monodisperse silica spheres in the micron size range, Colloid Interface Sci. 26 (1968) 62-69.

[48] N. Plumeré, A. Ruff, B. Speiser, V. Felmann, H.A. Mayer, Stöber silica particles as basis for redox modifications: particle shape, size, polydispersity, and porosity, J. Colloid Interface Sci. 368 (2011) 208-219.

[49] C.-F. Wang, F.-S. Tzeng, H.-G. Chen, C-J. Chang, Ultraviolet-durable superhydrophobic zink oxide-coated mesh films for surface and underwater-oil capture and transportation, Langmuir (2012) 10015-10019.

[50] M.-G. Jeong, H.O. Seo, K.-D. Kim, D.H. Kim, Y.D. Kim, D.C. Lim, Quenching of photocatalytic activity and enhancement of photostability of

ZnO particles by polydimethylsiloxane coating, J. Mat. Sci. 4 (2012) 5190-5196.

[51] R.P.S. Chakradhar, V.D. Kumar, J.L. Rao, B.J. Basu, Fabrication of superhydrophobic surfaces based on ZnO-PDMS nanocomposite coatings and study of its wetting behaviour, Appl. Surf. Sci. 257 (2011) 8569-8575.

[52] A. Klini, S. Pissadakis, R.N. Das, E.P. Giannelis, S.H. Anastasiadis, D. Anglos, ZnO-PDMS nanohybrids: A novel optical sensing platform for ethanol vapor detection at room temperature, J. Phys. Chem. C 119 (2015) 623-631.

[53] C. Yang, F. Wang, W. Li, J. Ou, C. Li, A. Amirfazli, Anti-icing properties of superhydrophobic ZnO/PDMS composite coating, Appl. Phys. A 122 (2015) 1-10.

[54] N.K. Neelakantan, P.B. Weisensee, J.W. Overcash, E.J. Torrealba, W.P. King, K.S. Suslick, Spray-on omniphobic ZnO coatings, RCS Adv. 5 (2015) 69243-69250.

[55] Personal email correspondence.

[56] K. Ichimura, S.-K. Oh, M. Nakagawa, Light-driven motion of liquids on a photoresponsive surface, Science 288 (2000) 1624-1626.

[57] S.-K. Oh, M. Nakagawa, K. Ichimura, Photocontrol of liquid motion on an azobenzene monolayer, J. Mat. Chem. 12 (2002) 2262-2269.

[58] H.B. Eral, D.J.C.M. ‘t Mannetje, J.M. Oh, Contact angle hysteresis: A review of fundamentals and application, Colloid Polym Sci. 291 (2013) 247-260.